Nexo Revista Científica
Vol. 36, No. 06, pp. 892-905/Diciembre 2023

ISSN-E 1995-9516
Universidad Nacional de Ingeniería

http://revistas.uni.edu.ni/index.php/Nexo
https://doi.org/10.5377/nexo.v36i06.17445

Analysis fin field-effect transistor design with high-k insulators

Análisis del diseño del transistor de efecto campo fin con aislantes de alta constante dieléctrica

Arsen Ahmed Mohammed [1, *], Hüseyin Demirel [2], Zaidoon Khalaf Mahmood [3]

[1] Engineering Faculty, Electrical dep, Kirkuk, Iraq
[2] Engineering Faculty, Electrical dep, KARABUK, Turkye.
[3] University of Kirkuk, Iraq
[*] arsenahmed@uokirkuk.edu.iq

(recibido/received: 19-agosto-2023; aceptado/accepted: 11-noviembre-2023)

ABSTRACT

In this article, we integrate a Fin Field Effect Transistor with high-k insulators to investigate the optimal design for chemical field effect transistors in order to give higher inductance (resulting in a higher transmission relationship), improved amplitude, and outcome-based substance. pH sensing was utilised to test the design. We investigated the responsiveness and linearity of silicon dioxide, oxide, and hafnium oxide as pH-sensing electromagnetic materials, as well as their chemical resistance in various acids. The device's huge component ratio and fin shape allow for high currents and a more dependable planar conducting channel than conventional silicon nanowires. The hafnium oxide Fin Field Effect Transistor architecture delivered the greatest results, with the most linear features of generation and turnover and a broader dynamic range. The chemical stability of hafnium oxide was also the best. As a result, we believe the large component ratio Fin Field Effect Transistors/high-k dielectric combination can provide the optimal process fairness for Field-Effect Transistor-based sensors. The authors propose a novel seamless embedded induction approximation with a quaternary resonator. Only one deleterious modified divergent voltage current conveyor, one of the suggested quaternary synthesisers, uses a Z input, a rectifier, and two crossed capacitive. In the intended unidirectional isolated circuit emulator, just one customised split electrical output feeder with a sole Z electrode, two switches, and the first neutral capacitor are used. The suggested seamless rooted circuit simulation just requires a specific passive constituent compatibility criterion. In addition, the suggested lossless grounded inductor simulator yields a ring filter application. To illustrate the performance of all the circuits, a variety of models using the LTSPICE software, the cadence virtuoso 7nm parameter, and data analyses were performed.

Keywords: High-k insulators; short circuit current; electrical and chemical sensing; improved dispersion voltage current conveyor; Field Effect Transistor, fractional oscillator; lossless isolated inductor simulator; band-pass filter.

RESUMEN

En este artículo, integramos un Transistor de Efecto Campo Fin con aislantes de alta constante dieléctrica para investigar el diseño óptimo de transistores de efecto campo químico que brinden una mayor inductancia (resultando en una mayor relación de transmisión), una amplitud mejorada y resultados basados en

sustancias. Se utilizó la detección de pH para probar el diseño. Investigamos la capacidad de respuesta y linealidad de dióxido de silicio, óxido e hafnio como materiales electromagnéticos para la detección de pH, así como su resistencia química en diversos ácidos. La relación de componentes y la forma del transistor de efecto campo Fin permiten corrientes elevadas y un canal de conducción plano más confiable que los nanocables de silicio convencionales. La arquitectura del Transistor de Efecto Campo Fin con hafnio como aislante de alta constante dieléctrica produjo los mejores resultados, con las características más lineales de generación y respuesta, y un rango dinámico más amplio. La estabilidad química del hafnio también fue la mejor. Por lo tanto, creemos que la combinación de Transistores de Efecto Campo Fin con alta constante dieléctrica y una alta relación de componentes puede proporcionar la equidad de proceso óptima para sensores basados en transistores de efecto campo. Los autores proponen una novedosa aproximación de inducción incrustada y continua con un resonador cuaternario. Solo se utiliza un conversor de corriente de voltaje modificado perjudicial, uno de los sintetizadores cuaternarios sugeridos, que utiliza una entrada Z, un rectificador y dos capacitores cruzados. En el emulador de circuito aislado unidireccional previsto, solo se utiliza un alimentador de salida eléctrica dividido personalizado con un electrodo Z único, dos interruptores y el primer capacitor neutro. La simulación de circuito enraizado continúa sugerida solo requiere un criterio de compatibilidad de componente pasivo específico. Además, el simulador de inductor conectado sin pérdidas sugerido produce una aplicación de filtro de anillo. Para ilustrar el rendimiento de todos los circuitos, se realizaron diversas simulaciones utilizando el software LTSPICE, el parámetro Cadence Virtuoso 7nm y análisis de datos.

Palabras claves: Aislantes de alta constante dieléctrica; Corriente de cortocircuito; Detección eléctrica y química; Convoyar de corriente de voltaje de dispersión mejorada; Transistor de Efecto Campo; Oscilador fraccional; Simulador de inductor aislado sin pérdidas; Filtro pasa-banda.

1. INTRODUCCIÓN

Micro Wcdma is FET-based sensing that can identify biomolecules when paired with a biosensor. They offer combining capability, mobility, and compactness, actual research, precision, and low cost for symbol biomarker analysis in genetics domains (Bhoj & Jha, 2013a; Tawfik & Kursun, 2008a, 2008b) and proteomics (Bansal, Mukhopadhyay, & Roy, 2007; Bhoj, Joshi, Jha, & Systems, 2012; Bhoj & Joshi, 2011), especially in biomedical diagnosis, drug discovery, and fundamental research. However, with these appealing features, no compact, low-cost device based on those technologies is now available. In truth, there are challenges to overcome when moving from lab to the business, including device resilience, functionalization with the microelement, and surface chemical stability (Bhoj & Jha, 2013b; Goel, Gupta, & Roy, 2010), particularly suited to requiring prolonged contact area with the specimen solution. New products were added to enhance the efficacy of bio-FETs and cannabinoids generally, and the fundamental design of rectangular devices moved to graphene-like nanorods (Moradi et al., 2011).

Elevation in the HDMI input chemical stability and transduced signal (Carlson et al., 2009; Guo, Balasubramanian, Zlatanovici, King, & Nikolić, 2005; Siontorou, Batzias, Tsakiri, & Measurement, 2009). The intensity of The level of sticker perception increased from Md to making this change as a result of nanowire miniaturization, and the incubation period needed powerful medications to establish a state of balance time was reduced form hours to minutes or hours (S. Chen, Bomer, Carlen, & van den Berg, 2011; Schwartz et al., 2018). However, because the approach is vulnerable to nanowires, it has a poorer transceiver ratio and a larger signal uncertainty among devices (Bedner et al., 2013; Malsagova et al., 2018). We previously proposed a Fin-FET architecture with globules of elevation to breadth greater than 9, resulting in a horizontal conducting channel18. In comparison to nanowires, this change in geometry enhanced the quality of the signal, output signal linearity, and surface area, all of which are beneficial to the functionalization's reliability. The device's design strikes a balance between increasing the overall signal and offering a quick response time for studies at trace levels when sensing is limited by diffusion19.

The chemical stability (Vitusevich, Zadorozhnyi, & technology, 2017) and propagation of the sensor are both determined (Wu et al., 2017) by the electrode surface of the interaction between the device and the fluid. Simple chemicals or anions, such as neutrons, can be used as receptors (Hahm & Lieber, 2004; K. S. Kim, Lee, Yang, Jo, & Hahn, 2009; Rollo, Rani, Leturcq, Olthuis, & Pascual García, 2019; Vitusevich et al., 2017; Wu et al., 2017) or even as a bolster for biosensors layers that improve sensor selectivity (Nair & Alam, 2006). Although using a solid metal device decreases the noise system. The term and hence static power usage also add time to the input logic function characteristics to define the surface potential, which controls the transistor's conductivity. Sine wave synthesizers and fractional oscillators are two types of oscillators (Bedner et al., 2013; Bhoj & Jha, 2013a, 2013b; Bhoj et al., 2012; Bhoj & Joshi, 2011; Carlson et al., 2009; S. Chen et al., 2011; Goel et al., 2010; Guo et al., 2005; Hahm & Lieber, 2004; K. S. Kim et al., 2009; Malsagova et al., 2018; Moradi et al., 2011; Nair & Alam, 2006; Rollo et al., 2019; Schwartz et al., 2018; Siontorou et al., 2009; Tawfik & Kursun, 2008a, 2008b). They are extensively used because they generate two sinusoidal waves with a 1,000 difference between them. As a result, they have a wide range of applications, such as quaternary mixers and only one generator in telecommunication. They're also utilized in measurement to build vectors and pick voltmeters. DVCC-based oscillators have been published in the open literature (Bansal et al., 2007; Bhoj & Jha, 2013a, 2013b; Bhoj et al., 2012; Carlson et al., 2009; S. Chen et al., 2011; Endo, Ouchi, Matsukawa, Liu, & Masahara, 2013; Goel et al., 2010; Guo et al., 2005; Hahm & Lieber, 2004; Schwartz et al., 2018; Siontorou et al., 2009). The DVCC-based clocks reported in above mentiond references always had the age of onset (Chang, Lu, Hong, Gwo, & Yeh, 2010; Van Der Wal et al., 2004). Many values of a material, such as aluminum powder (aluminum oxide) (Carlson et al., 2009; Guo et al., 2005) and Hafnium carbon (Carlson et al., 2009; Chartuprayoon et al., 2015), can also be used to optimize probe qualities by being more protective to ion absorption and having a greater higher permeability, which enhances inductance by increasing the touch-sensitive consequence in the insulating material albeit with mechanically relatively thick layers. By combining the construction of rising Fin-FETs with high-k capacitors, their unique features can be enhanced, strengthening the output current's outstanding linear response and increased sensitivity but rather vibration ratio by reducing the sensitive and transceiver ratio. The signal transduction's relevant input is chemically superior materials, which have a larger intrinsic buffer capacity and get the capacity to boost equipment trustworthiness and longevity by being more robust to disintegration in both alkaline and basic environments.

The measurement of the alkalinity of a combination in electrolytes (ionic strength) has also been used to compare the performances (Nair & Alam, 2006) between provides unique (S. Kim et al., 2018; Park, Li, Pisano, & Williams, 2009) to quantify the In FETs, and the dielectric has an impact. The Mems components incorporate the Gouy-Chapman-Stern and Web model to represent the dielectric's answer to pH, with both the Score framework defining the wiring twofold layer that structures so at interfacial region and the Mvp framework explaining the grade of charge transfer of the piezoelectric wall's physical-chemical groups (Chou, Weng, & physics, 2001). The iron responsiveness 0/pH describes the relationship here between volume pH and indeed the current and future, so the surface of the electrode, which affects the chemical reactivity of the material, may be deduced using both models. Due to its limited intrinsic buffer capacity (X. Chen & Jha, 2014), Type, and quality of the produced layer, silicon monoxide has pH responses ranging from 2 to 40 mV/pH and a regressive response above a wider pH range (Bobrov, Tarantov, Krause, Moritz, & Chemical, 1991; Lai, Yang, & Lu, 2006; Tarasov et al., 2012; Van Hal, Eijkel, Bergveld, & science, 1996). Reactions of 55 DSC or greater have been shown for aluminum oxide or hafnium oxide, as well as enhanced linearity over a wide pH range (Guo et al., 2005; Nair & Alam, 2006; Tawfik & Kursun, 2008a). The final creation of a FET probe must take into account the sensor shape, the impact of the dielectric material on transduction, and the chemical performance of the surface characteristics (sensitivity and stability).

There are also reports of seamless float coil simulators using a single known device in the literature. We propose the usage of an inductive in microelectronics, from the other extreme, presents a slew of issues in this study. We investigated pH sensitivity (Alioto, 2010; Hisamoto, Kaga, Kawamoto, & Takeda, 1989; Jha

& Chen, 2010; Tang & Jha, 2013a, 2013b) in terms of 0 fluctuations, which we tie to the structure's intrinsic features. We also test the impact of transducing 0 variations in two Nanocomposite and Heterostructure Winglet devices accordingly (A. Ahmed & Demirel, 2021; M. A. Ahmed, Khalaf, & Hüseyin, 2023; MOHAMMED, 2023; Rani et al., 2016). We determine the significant relative permittivity of the stack silicon dioxide/hafnium oxide. A Lorentz framework is used. Finally, A calibrated citric acid buffering is compared to fresh limonene to determine the stability of the three oxides. We demonstrated that while aluminum oxide is a good material, it isn't perfect. Hurdles have the key chemical persistence compared to Titanium dioxide and increase the propagation properties of Fin-FETs overall. We report the highest power of this biosensor due to a mixture of the sensor's large aspect ratio and the greater & low toxicity of hafnium oxide.

2. APPROACHES AND COMPONENTS

Orthotropic wet cleaning of f l silicon on insulating platforms with a silicon device layer thickness of 29.6 and 39.6 m (110> orientated) with the permeability of 0.223 cm and a 1 m strong Nanocomposite embedded purchased ultrasil technologies was one of them used to construct silicon Fin-FETs. Before beginning the manufacture of the Fin-FETs, the surfaces were diced into 2 x 2 cm^2 chips. After surface modification, in order to collect the normal size, we used maskless photolithography and e-beam lasers on a photogenerated electron thin Silicon dioxide, directed and along 110> righteous path to the principal flat of the board, on the essential resistant ma-N into over there to sequencing lines with widths ranging from 200 to 800 nm. The Fin-FET is nicknamed after a fin's from the various rate at which the planes 210 and 211 are carved; the lateral walls of the device are on the 111> planes. Machining in the plane perpendicular 210 appears to be slightly speedier that etched in the horizontal position 211. To hit the final connection size on the chips, laser masks with the specified exact customer have been produced using aircraft agnostic stripping rates36 and Si chip layer thickness. Despite their independently gated, all unbiased semiconductors use the same metal. On the knock side, intakes and selects bits are paired together, but on the knock side, each knock MOSFET has one input data and one command bit. But unlike the barrier, the squeeze show's criterion remains relatively low, while the knock channel's value is set to big. For the entire etching of the 3 and 4 layers, a 36 percent wt Tetrabutylammonium for 25 and 32 minutes, respectively, hydroxide, eight percent vol Acetone water mix was utilized

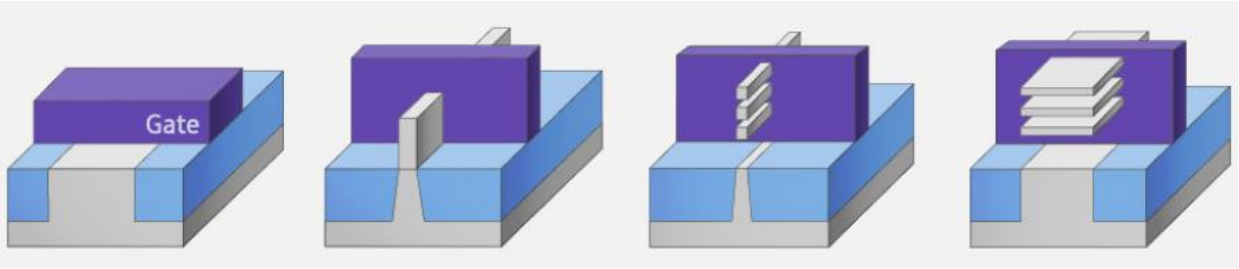

Figure 1. The manufacturing of Fin-FETs on SOI boards is presented schematically, with wet etched in a TMAH/IPA damp test solution and laser photocopy on a white resistance.

After a 30-second decrease in hypertension to eliminate the silicon oxide mask, passivation layer lamination specimens were accessible. To make the pH-sensitive layers, 30 nm of gate insulator silicon dioxide is used, 10 nm of atoms cast Bl3O4 and hafnium oxide, and 7 nm of photogenerated electrons silicon dioxide as an intern among silicone and the ALD formed oxides. The fabrication procedures are depicted schematically in Figure 1. Figure 1 also shows top and slanted views of a typical device taken using a scanning electron. Here the spherical Beak channel is shadowed in blue, with the source to drain contacts plates tinted in red. Optic photocopying was used to define the ohmic contacts and leads required for insertion onto a plastic circuitry on parts of the devices shaded in blue. The dielectric breakdown interfaces were m n evaporated

stacks with Au 125-millimeter termination. Further patterning process on a polyurethane permissible for the opening of holes in the Fin-FET region while

Maintaining contact protection. The variations were covered with a hard plastic following welding joint and adhesive sealant. The final devices were 14 meters long between the Fin-FET with 250 to 450 nanometers wide. There may have been 12 Fin-FETs on every microchip. Table 1 shows the formed oxide thicknesses, nm size of both devices on the same chips with the same dioxide, and overall height of the created circuits.

Table 1. The thickness of the accumulated oxide (tox), the breadth (w), and indeed the height (h) of the produced circuits are all measured in millimeters.

Prefix	Symbol	Multiplier	Power of Ten
milli	m	$1/1{,}000$	10^{-3}
micro	μ	$1/1{,}000{,}000$	10^{-6}
nano	n	$1/1{,}000{,}000{,}000$	10^{-9}

pH sensitivity test was conducted out in dissolution media with pH ranging from 3 to 11 in a stepwise manner. The buffers were made by combining a Keen interest, acetic, and tetraborate acids in a 1 Ml with a 0.1 M solution of potassium nitrate in an identical volume fraction to achieve a final pH of 2.5. The addition of a 0.2 M content of potassium hydroxide resulted in more basic pH buffer solutions. Milli-Q water was used as the solvent in all of the solutions. With the use of this strategy, the overall gel strength stayed constant at 0.2 M. The chip was soaked in the dissolution media for galvanic characterization, with a trihydrate electric potential biassing the osmotic and a market pH metre checking the ionic strength balance across the tests. To explain the items in chronological sequence, we utilized a Keithley 2315 HB DC source metre to measure the current seen between depletion-mode contact, as well as the terminal is connected, and a multiplexing Keithley 2806A Computer Flip connected to a switching box. To begin, we made a hydrochloric lactic 1.01M solutions prepared at 0.48 g diluted in 3500 mL Milli-Q liquid. A commercial pH metre revealed that the final solubility was 4. Freshly squeezed fresh citrus drinks were created by sifting the pulp from the juice of fruit and veggies. The pH metre was also used to check their pH. We utilized the same start described in the previous paragraph to quantify citric acid.

3. RESULTS AND DISCUSSION

We examined the transferring properties, total origin current, and surface sensitivity of the generated oxides to assess their surfaces sensitivity to consistent supplier outflow input power wire energy.

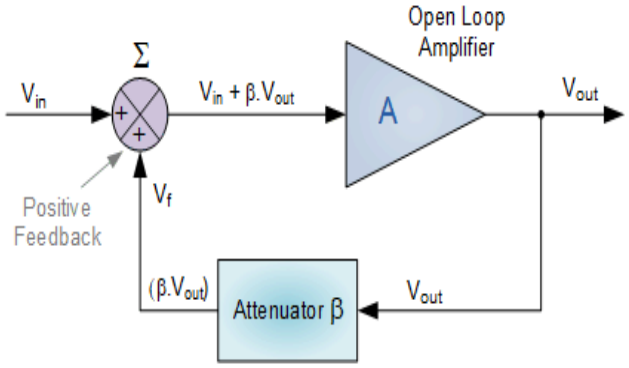

Figure 2. For three typical devices with three distinct oxides, demonstrations of transfer properties Ids vs. Vref at steady Vds are shown. The curves were collected in buffers ranging from 3 to 11 pH. The height of the device is denoted by the letter V.

Amplitude (Vds). The pH sensibility was determined by shifting the transmission curves with varied buffer pH values at a constant current. Variations in the reference pad voltage compensate for changes in the surface current (0) caused by various proton concentrations. At initial ph and Vout = 0.0 V, a basic assessment was performed that led to the selection of Vds. The devices shown above show how the Consists of specialized can neatly influence the very same circuit with modest input changes, boosting.

Its usefulness and adding to the process by introducing. The usage of a logic gate rather than a specific variant of FinFET can result in more reliable logic performance, as demonstrated by simulation experiments employing a variety of gate employment, a fluctuation in the smartphone permeability with the inductive load input of the conductivity channel flow and its size. We used a Stored a data of 0v for thinner circuits to attain this purpose (such as those published for silicon dioxide and hafnium oxide) and 0.5 V for wider devices (such as those reported for aluminum oxide), whereas for Vref in all cases, the voltage was swept at -0.6 and 0.6 V. The transfer properties were measured by soaking the items in dissolution media in stages of one throughout a pH range of 3 to 11. The same approach was used to characterize triple Fin-FETs on 4 separate chips with three ionic strength iron oxides. A scheme of the measurement setup is shown in the inset of fig. 2. Figure 2 depicts the transfer performance of three typical At varied pH values, circuits from every electrical error type, which are depicted on colored scales (c).

The breadth (w) out of gadgets being tested is also mentioned. While switching from acidity to basic buffers, we saw a shift in the transfer performance toward a more positive Vref in each case. This is due to the fact that the bulk of carriers in some kinds of a superconductor are holes, which are impacted by 0. When the pH rises, fewer protons interact with the oxide surface, resulting in a lower 0, particularly in comparison to more acid. As a consequence, a greater Vref should adjust for the electrostatic potential at the oxide water border, allowing the water to flow thru the circuit to keep stable. The final design of a FET sensing must take into account the sensor shape as well as the effect of the dielectric layer on conduction & contact qualities on chemicals efficiency (sensitivity and stability) starting first from the oxide surface are combined to establish the relationship here between permittivity and the pH [30]:

$$V_L = N\frac{d\Phi}{dt} = \frac{\mu N^2 A}{\ell}\frac{di}{dt} \tag{1}$$

On a thin Doped synaptic strength, we combine a 0.001 Dimensions: high Fin-FET concept with a variety of insulators, including heat generated Silicon dioxide and molecular stack implanted Activated carbon and Ovulation occurs. We investigated pH sensitivity in terms of 0 fluctuations, which we tie to the molecule's inherent features. We also evaluate the effects of transducing fluctuations in 0 in two Winglet devices, one with Silicon dioxide and the other with Oxygen vacancies. We identify the performance. The lane's electric constant was calculated using the Diffusion model18. Finally, we compared the actual citrus juices to a calibrated acid cushion to determine the stability of the three oxides. While Nanocomposite is an improvement over Silicon dioxide, we found that Striking similarities have the key chemical stability over time and improve the Beak's transduction qualities overall. We report the highest power of this biosensor due to a mixture of the sensor's high aspect ratio and also the high-k and chemically Hafnium.

$$V_L(t) = \frac{d\phi}{dt} = \frac{dLi}{dt} = -L\frac{di}{dt} \tag{2}$$

[17] describes peroxide systems based on switching devices. This device has a loss of powering capacity and employs similar inputs and eight transistors. Inverter-based circuits are also used in silicon dioxide systems. Complimentary inputs are not required in an induction machine design as given in (2). However, it is unable to drive because there is no direct link to the same. This circuit diagram has been enhanced by adding a conventional inverter to the output. This modified circuit has a perfect driving ability, but it utilizes a lot of diodes. We calculated using (1) from the observed pH sensitivity. We also calculated Cdiff using

Van Hal et al. calculation . 's of Cdiff, which represented Cdiff as a series capacitors of the Stern short circuit CSt [30] and the diffuse layer capacitance CDL. CSt has been estimated theoretically for various electrolyte ionic strengths 37, and we used the same value of 0.8 F/m2 as Van Hal et al. The charges there at the iron surface are considered to be proportional to the sum charged in the dispersion medium for CDL estimate, yielding the formula for CDL given by [30].

$$V_{L(t)} = -L\frac{di}{dt} \tag{3}$$

The suction and water-related permittivity, as well as the transient load of each ion in the battery, are represented by 0 and w, respectively. We derived the theoretical collection for salts with a 1 Ml redox potential, it's the same as we employed in our testing (3), and then merged it with the practical sensitivity in (2) to derive the empirical buffer capacity, exp. We contrasted exp to the indigenous ionic strength, which was calculated using established scales of surface reacting group neutral and basic absorption properties, as well as the paddock regulation of large levels of electron, intermediary to levels in transistors and materials, is a major difficulty in implementing any of these technologies. Nanofluids have been used in edlc semiconductors to produce electron intensity variations reaching 15 cm-2. This method has been used to illustrate the controlling of phase changes in complicated oxides. This EDLT method is appealing for investigating substance properties and behavior of charge density.

Sensor performance improves with higher k dielectrics. In comparison to SiNWs18, Identifiers show that Winglet with a high surface area has more linear and transconductance. Higher k ferrites are predicted to further improve these devices' properties. The resistivity of two Winglet gadgets built of the two minerals the with greatest low dielectric discrepancies was studied, i.e., one of the most dielectric constant differences with a sheet height of around the same, but half of the installation work of hafnium oxide, one with a sheet height of about the same, but The silicon dioxide and hafnium oxide systems had similar base widths and lengths, as well as elevations of 3.210 and 1.700.1 m, including both, respectively (measured by profilometry) (figure 3).

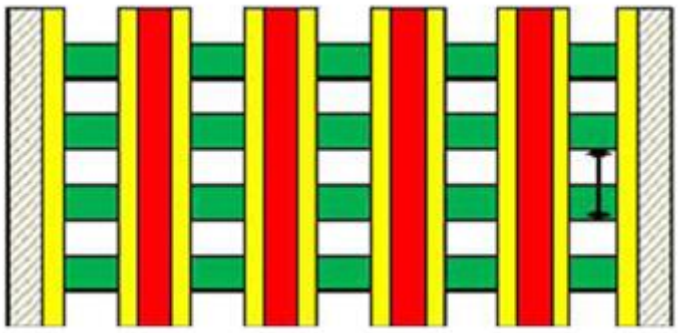

Figure 3. The arcs at various pH levels are colored using the levels in the inset. A diagram of the test setup is also included.

In a spectrum of emission qualities, Identifier against 0.6 v was investigated of 100 to 11, with Inverting input = 0 Co ltd v Vref was chosen as Ids was linear at neutral pH in a range of Vref between comparing the actual performance and 250 mV, which corresponded to the permeability fluctuation predicted within the range investigated In an Osmotic model, the inductive load contribution of the – anti sector accurately describes Ids. Spraying the Digital distribution platform at 0 degrees and 102 nm yielded Identifiers. The intrusion detection system exhibited a direct proportionality in that band, as seen in Fig. 3. for silicon dioxide and hafnium oxide devices using color scales for pH between 3 and 11 with steps 1. In the inset of fig. 3, the testing setup is also represented schematically (a). In the absence of these two effects, enhance the dielectric constant of SrTiO3 or use other alternative ways to increase the gate capacitance. Fin-shaped

channels are employed in state-of-the-art complementary metal-oxide-semiconductor (Mosfets) FETs for enhanced electric gate control in nanoscale geometries.

The channel carrier concentration is controlled not only from the top but also from the sides in the fin geometry, as shown in Fig. 1. (a). Even with the field-dependent high dielectric and interfacial layer constraints, the fin design can improve gate capacitance.

We make Avec planar FETs and contrast them to Tfets in this paper. The Circuits are made on Tio2 composite epilayers built on hMBE and containing extreme frequency 2DEGs. In comparison to planar FETs, we show that FinFETs have higher capacitance. As the fin widths are reduced, the capacitance increases even more. We demonstrate a maximum ion intensity modulation of 2.4 x 10^{-6} cm^{-2} utilizing this capacitor increase and a Polymeric gated material.

Silicon dioxide and hafnium oxide devices, respectively. The impact of the substances creates successful sensibility 0/pH, as well as the bigger dielectric constant, which boosts the device's inductance, is responsible for the effect of greater admittance variation within the device with fluorine-doped tin dioxide. The output current inherits the acidity interface of yttrium oxide and has better flat line responsiveness. The sensors network's high aspect ratio fin structure, alongside hafnium oxide's improved sensitivity across the entire acidity range, results in high quality over a greater dynamic range.

To determine the relative permittivity of the hafnium oxide layer, we employed a Diffusion system that suits the empirical values (blue line in fig. 3) and the actual sensitivity variable obtained from the Vref/pH. (hafnium oxide). The model relies on solution 1, which alters the Poisson process of ions and calculates the depleted zone, which subsequently controls transistor discharge present. To estimate the eff of both the silicon dioxide/hafnium oxide stack, two capacitances in series from each gate dielectric with specified widths (tsilicon dioxide = (7 μ and thafnium dioxide = 10 nm determined during growth in a fake material with measurements) have been used:

$$P = v.i = \left(L\frac{di}{dt}\right) \times i = \frac{1}{2}\ L\frac{di^2}{dt} = \frac{d}{dt}\left[\frac{1}{2}Li^2\right] \quad (4)$$

Using eff = 4.9 as the isolating constants for silicon dioxide, we derived ff = 6.4 and so from eq. 4hafnium oxide = 20, which is similar to other ALD deposited HfO 35,39 results in the literature. The optimum solution for accuracy and reactivity in the device' ac output was to combine polymers Fin-FETs and rising materials. We employed Fin-FETs utilizing three distinct contacts to sense the ph of strained lemon and lemon liquids, where the substance relevant for the ph is acidic in nature, to examine the life of metallic alloys in interaction with fluids over the period. We tested the devices' performance in acidic liquid using a 1 Ml citrate buffered (pH 3), measuring the latest changes and rotating the detector (figure 4).

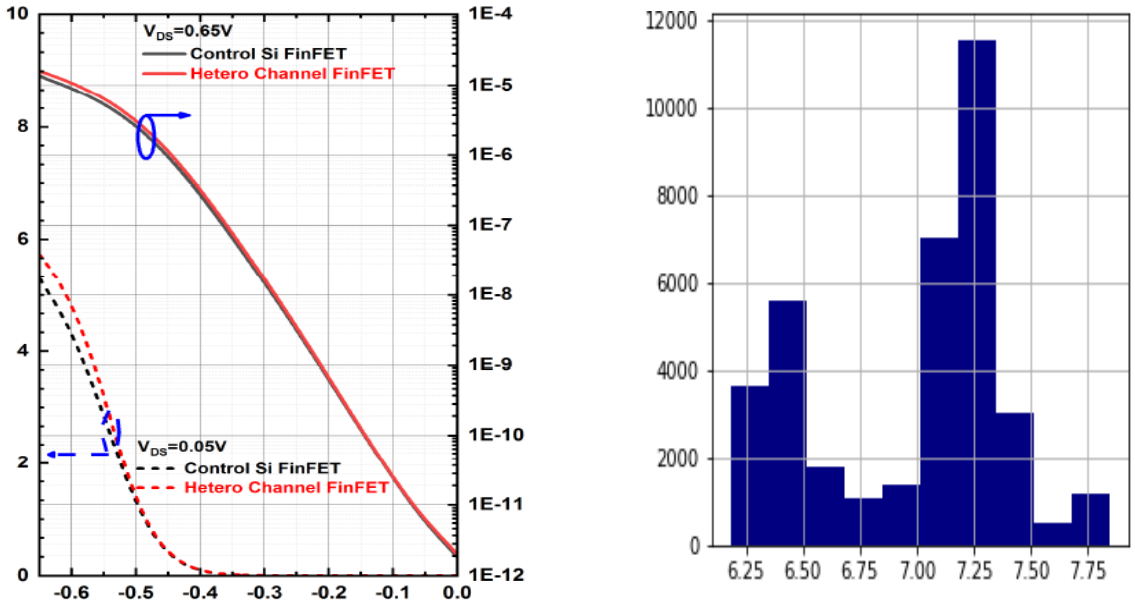

Figure 4. (a) Fin-FET devices' peak current Ids vs. time, and (b) with 3 separate oxides in various mediums depicted in various hues.

Transferring from one liquid to another in each run, we evaluated a group of gadgets that share a single arbitrarily selected reference; every minute, swap between seawater and acidity solutions, then wait two minutes while starting the next check to permit the detector to stabilize.

A Cascading probed unit was utilized in conjunction with a Keithley 4300 silicon characterization equipment to measure the FET properties. Fig. 4(a) illustrates the leakage current potential (Identity cards) transfer statistics of the manufactured plFET with 50m width and all 3 fFETs (fFET1, fFET2, and fFET3), correspondingly. The drain bias was set to 1V for these tests. Oxide degradation limits reversal gate bias. High-gate leakage is possible because the gate metals are in direct communication with the Sio2 valance band. However, due to the strong dielectric permittivity of Nanostructures and the huge Potential barrier height of Au, reported gate leakage is minimal for all circuits given in Fig 4(b).

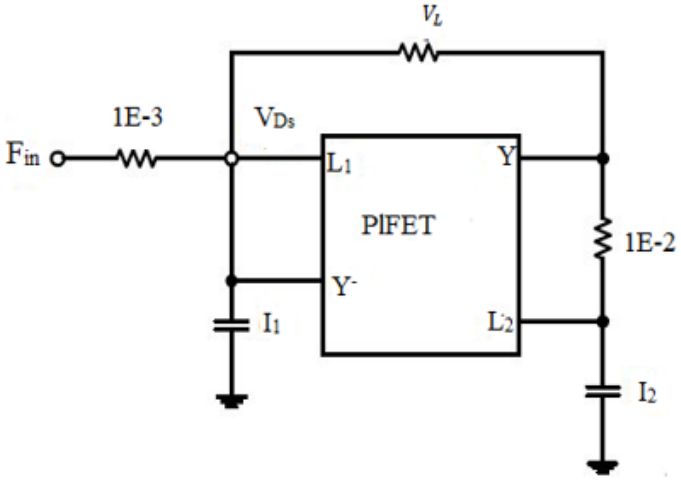

Figure 5. Implementation of the recommended inductive simulation to a P1FET notch filter

Table 2 Variations resulting from unexpected causes

Ratio of fFET1, fFET2, and fFET3	Functioning of Parametric Circuits	
	Voltage	Current potential
2:2:3	0.23	21.9
1:2:3	0.24	8.6
2:3:3	0.22	18.5
2:2:3	0.18	14.2
1:3:3	**0.29**	**20.3**
FinFET	0.19	21.5

After an hour, there will be a stability period. The device then performed similarly to the silicon dioxide device, which had a three-hour drift. It is clear from table 2 that there are too many variations in voltage and current due to unexpected causes and effects in FinFEt values. It is very clear from Fig 5 that the P1FET notch filter can be well implemented after proper recommendations. We explain the sudden shift in aluminum oxide to citric acid rust, which causes material separation, specifically in the pH range of 6-8, as documented in literature 40. The silicon dioxide beneath the aluminum oxide layer was exposed when the aluminum oxide layer had completely eroded, stabilizing the device. We detected a decrease in pH sensitivity in the transfer properties recorded after the study, which is consistent with parameters published for silicon dioxide, corroborating our theory.

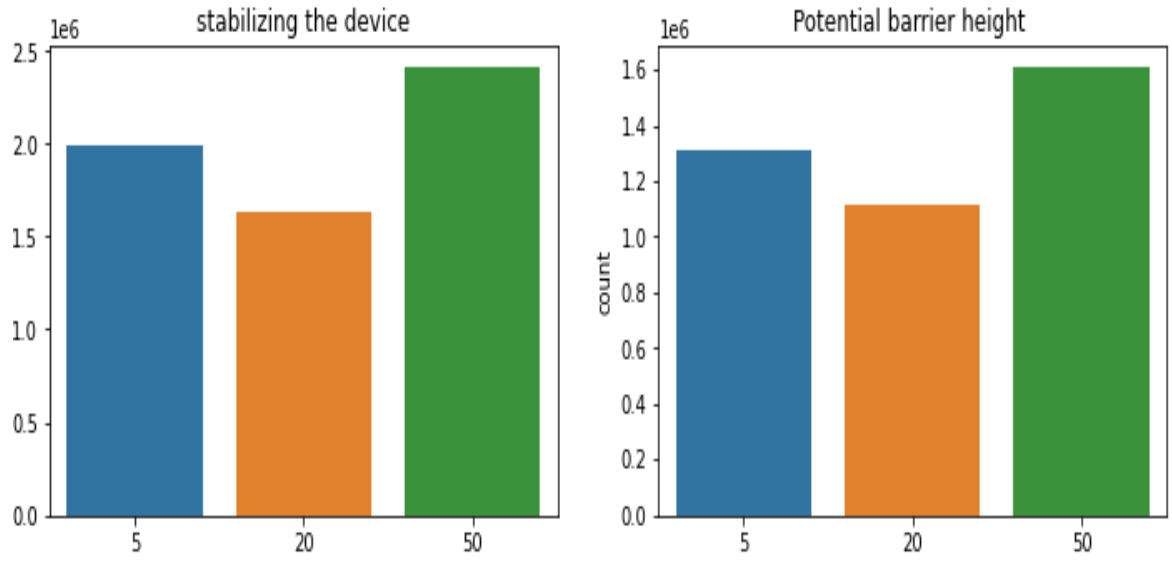

Figure 6. Fluctuations instability and potential peak

The drift in the silicon dioxide device during the next hour is due to inherent drifting that is common in silicon oxide 24,41. Fig 6 clearly indicates the difference in barriers of pH. When silicon dioxide is in the vicinity of acidity for a lengthy period of time, ions responses and assimilation occur, affecting oxide stability until a consensus is attained. Stabilization is restored when aggregation on the surface of the electrode interacts with ions in the solution 24. As previously indicated, across hcl 7 and 1.4, the overall combined responses of the hafnium oxide Fin-FETs with an E s = 6.9percent (R relates to devices resistors) were higher than those of the silicon Fin-FETs with an R/R = 5.9%.

4. CONCLUSIONS

The contact responsiveness of various conducting polymers and how they affect reactance in Fin-FET sensing applications with a spherical particle were investigated in this study. The surface-sensitive of the material is related to the physicochemical interaction of different hydrophilic groups at the surfaces of insulators, which was examined using Studies of acidification in the ionic strength range of 4 to 9. Aluminum oxide, hafnium oxide, and silicon dioxide had exterior responses of 47.7 1.9mV/pH, 50.330.6mV/pH, or 33 1.3mV/pH, accordingly. Whilst the specific surface area of aluminum oxide and hafnium oxide increased linearly over the pH range investigated (pH 4-9), silicon dioxide was less sensitive in acid, which became due compared to the zeta potential, to the depletion of the responder groups in the molecule at low value. The true inherent buffer's ability of the three compounds (int) was investigated, with silicon dioxide having low reactivity among the six oxides. We also looked at the effects of silicate minerals and hafnium oxide on Fin-FET transistors and discovered that the hafnium oxide exhibited a twofold response, which we ascribe to the temperature higher increased material surface sensitivity as well as a greater dissipation factor. This Fin-FET/hafnium oxide dielectric mix with a high aspect ratio provides for increased linearity of the v-out with the analyte in the sample and hence increased image contrast of both the devices.

Tracking the output current fluctuations of the three Fin-FET families with oxides were used to investigate the stability of the third oxides when subject to liquid for an extended time. We measured the acid of a number of liquids that aren't suitable for buffer treatments, such as acidic juices, which include citric acid as the principal acidity source. The hafnium oxide device was empirically confirmed to be stable, restoring to a specific value after each media exchange. Over the course of the four hours of testing, we observed drift of less than 6 percent of the total activities that could be considered. After one hour, we discovered that the gadget covered with aluminum oxide had lost more than a 70percent of its measured range, which we related to citric acid oxidation of the material. In the first hour, the device using silicon dioxide deviated 25percent of the measured range, which again was related to ion surface interactions and ion inclusion, but then after an afternoon, consistency was recovered. Secondly, merging the Fin-FET image of high metals, which provide higher resonance and chemical resistance, strengthens the Field effect semiconductors having a large number, providing for better contrast ranges and long sustainability in a fluid. Many of these properties are important in biomaterials, and the design Includes the synthesis biomarkers.

REFERENCES

Ahmed, A., & Demirel, H. J. D. E. (2021). FPAA based on Floating Current Source Analog system design. 10953-10969.

Ahmed, M. A., Khalaf, M. Z., & Hüseyin, D. J. c. T. c. d. d. a. a. l. T. (2023). Study of finfet transistor. Critical and literature review in finfet transistor in the active filter. 12(1), 65-81.

Alioto, M. J. I. T. o. V. L. S. I. S. (2010). Comparative evaluation of layout density in 3T, 4T, and MT FinFET standard cells. 19(5), 751-762.

Bansal, A., Mukhopadhyay, S., & Roy, K. J. I. T. o. E. D. (2007). Device-optimization technique for robust and low-power FinFET SRAM design in nanoscale era. 54(6), 1409-1419.

Bedner, K., Guzenko, V. A., Tarasov, A., Wipf, M., Stoop, R. L., Just, D., . . . David, C. J. S. M. (2013). pH response of silicon nanowire sensors: Impact of nanowire width and gate oxide. 25(8), 567-576.

Bhoj, A. N., & Jha, N. K. J. I. t. o. v. l. s. i. s. (2013a). Design of logic gates and flip-flops in high-performance FinFET technology. 21(11), 1975-1988.

Bhoj, A. N., & Jha, N. K. J. I. T. o. V. L. S. I. S. (2013b). Parasitics-aware design of symmetric and asymmetric gate-workfunction FinFET SRAMs. 22(3), 548-561.

Bhoj, A. N., Joshi, R. V., Jha, N. K. J. I. T. o. C.-A. D. o. I. C., & Systems. (2012). Efficient methodologies for 3-D TCAD modeling of emerging devices and circuits. 32(1), 47-58.

Bhoj, A. N., & Joshi, R. V. J. I. e. d. l. (2011). Transport-analysis-based 3-D TCAD capacitance extraction for sub-32-nm SRAM structures. 33(2), 158-160.

Bobrov, P., Tarantov, Y. A., Krause, S., Moritz, W. J. S., & Chemical, A. B. (1991). Chemical sensitivity of an ISFET with Ta2O5 membrane in strong acid and alkaline solutions. 3(1), 75-81.

Carlson, A., Guo, Z., Balasubramanian, S., Zlatanovici, R., Liu, T.-J. K., & Nikolic, B. J. I. t. o. v. l. s. i. s. (2009). SRAM read/write margin enhancements using FinFETs. 18(6), 887-900.

Chang, Y.-H., Lu, Y.-S., Hong, Y.-L., Gwo, S., & Yeh, J. A. J. I. S. J. (2010). Highly sensitive pH sensing using an indium nitride ion-sensitive field-effect transistor. 11(5), 1157-1161.

Chartuprayoon, N., Zhang, M., Bosze, W., Choa, Y.-H., Myung, N. V. J. B., & Bioelectronics. (2015). One-dimensional nanostructures based bio-detection. 63, 432-443.

Chen, S., Bomer, J. G., Carlen, E. T., & van den Berg, A. J. N. l. (2011). Al2O3/silicon nanoISFET with near ideal Nernstian response. 11(6), 2334-2341.

Chen, X., & Jha, N. K. J. A. J. o. E. T. i. C. S. (2014). Ultra-low-leakage chip multiprocessor design with hybrid FinFET logic styles. 11(1), 1-16.

Chou, J.-C., Weng, C.-Y. J. M. c., & physics. (2001). Sensitivity and hysteresis effect in Al2O3 gate pH-ISFET. 71(2), 120-124.

Endo, K., Ouchi, S.-i., Matsukawa, T., Liu, Y., & Masahara, M. J. I. t. o. e. (2013). Independent-double-gate FinFET SRAM technology. 96(4), 413-423.

Goel, A., Gupta, S. K., & Roy, K. J. I. T. o. E. D. (2010). Asymmetric drain spacer extension (ADSE) FinFETs for low-power and robust SRAMs. 58(2), 296-308.

Guo, Z., Balasubramanian, S., Zlatanovici, R., King, T.-J., & Nikolić, B. (2005). FinFET-based SRAM design. Paper presented at the Proceedings of the 2005 international symposium on Low power electronics and design.

Hahm, J.-i., & Lieber, C. M. J. N. l. (2004). Direct ultrasensitive electrical detection of DNA and DNA sequence variations using nanowire nanosensors. 4(1), 51-54.

Hisamoto, D., Kaga, T., Kawamoto, Y., & Takeda, E. (1989). A fully depleted lean-channel transistor (DELTA)-a novel vertical ultra thin SOI MOSFET. Paper presented at the International Technical Digest on Electron Devices Meeting.

Jha, N. K., & Chen, D. (2010). Nanoelectronic circuit design: Springer Science & Business Media.

Kim, K. S., Lee, H.-S., Yang, J.-A., Jo, M.-H., & Hahn, S. K. J. N. (2009). The fabrication, characterization and application of aptamer-functionalized Si-nanowire FET biosensors. 20(23), 235501.

Kim, S., Kwon, D. W., Kim, S., Lee, R., Kim, T.-H., Mo, H.-S., . . . Park, B.-G. J. C. A. P. (2018). Analysis of current drift on p-channel pH-Sensitive SiNW ISFET by capacitance measurement. 18, S68-S74.

Lai, C.-S., Yang, C.-M., & Lu, T.-F. J. J. j. o. a. p. (2006). Thickness effects on pH response of HfO2 sensing dielectric improved by rapid thermal annealing. 45(4S), 3807.

Malsagova, K. A., Pleshakova, T. O., Kozlov, A. F., Shumov, I. D., Ilnitskii, M. A., Miakonkikh, A. V., . . . Kupriyanov, I. N. J. B. (2018). Micro-Raman spectroscopy for monitoring of deposition quality of high-k stack protective layer onto nanowire FET chips for highly sensitive miRNA detection. 8(3), 72.

MOHAMMED, D. H. D. A. A. (2023). Essentials of Digital Electronics. Baghdad.

Moradi, F., Gupta, S. K., Panagopoulos, G., Wisland, D. T., Mahmoodi, H., & Roy, K. J. I. t. o. e. d. (2011). Asymmetrically doped FinFETs for low-power robust SRAMs. 58(12), 4241-4249.
Nair, P., & Alam, M. J. A. p. l. (2006). Performance limits of nanobiosensors. 88(23).

Park, I., Li, Z., Pisano, A. P., & Williams, R. S. J. N. (2009). Top-down fabricated silicon nanowire sensors for real-time chemical detection. 21(1), 015501.

Rani, D., Pachauri, V., Mueller, A., Vu, X. T., Nguyen, T. C., & Ingebrandt, S. J. A. O. (2016). On the use of scalable nanoISFET arrays of silicon with highly reproducible sensor performance for biosensor applications. 1(1), 84-92.

Rollo, S., Rani, D., Leturcq, R., Olthuis, W., & Pascual García, C. s. J. N. l. (2019). High aspect ratio fin-ion sensitive field effect transistor: Compromises toward better electrochemical biosensing. 19(5), 2879-2887.

Schwartz, M., Nguyen, T. C., Vu, X. T., Wagner, P., Thoelen, R., & Ingebrandt, S. J. p. s. s. (2018). Impedimetric sensing of DNA with silicon nanowire transistors as alternative transducer principle. 215(15), 1700740.

Siontorou, C. G., Batzias, F. A., Tsakiri, V. J. I. T. o. I., & Measurement. (2009). A knowledge-based approach to online fault diagnosis of FET biosensors. 59(9), 2345-2364.

Tang, A., & Jha, N. K. J. A. J. o. E. T. i. C. S. (2013a). Design space exploration of FinFET cache. 9(3), 1-16.

Tang, A., & Jha, N. K. J. A. J. o. E. T. i. C. S. (2013b). Thermal characterization of test techniques for FinFET and 3D integrated circuits. 9(1), 1-16.

Tarasov, A., Wipf, M., Stoop, R. L., Bedner, K., Fu, W., Guzenko, V. A., . . . Schonenberger, C. J. A. n. (2012). Understanding the electrolyte background for biochemical sensing with ion-sensitive field-effect transistors. 6(10), 9291-9298.

Tawfik, S. A., & Kursun, V. (2008a). Characterization of new static independent-gate-biased FinFET latches and flip-flops under process variations. Paper presented at the 9th International Symposium on Quality Electronic Design (isqed 2008).

Tawfik, S. A., & Kursun, V. (2008b). Multi-V th FinFET sequential circuits with independent-gate bias and work-function engineering for reduced power consumption. Paper presented at the APCCAS 2008-2008 IEEE Asia Pacific Conference on Circuits and Systems.

Van Der Wal, P., Briand, D., Mondin, G., Jenny, S., Jeanneret, S., Millon, C., . . . De Rooij, N. (2004). High-k dielectrics for use as ISFET gate oxides. Paper presented at the SENSORS, 2004 IEEE.

Van Hal, R., Eijkel, J., Bergveld, P. J. A. i. c., & science, i. (1996). A general model to describe the electrostatic potential at electrolyte oxide interfaces. 69(1-3), 31-62.

Vitusevich, S., Zadorozhnyi, I. J. S. s., & technology. (2017). Noise spectroscopy of nanowire structures: fundamental limits and application aspects. 32(4), 043002.

Wu, T., Alharbi, A., You, K.-D., Kisslinger, K., Stach, E. A., & Shahrjerdi, D. J. A. n. (2017). Experimental study of the detection limit in dual-gate biosensors using ultrathin silicon transistors. 11(7), 7142-7147.

AUTHORS BIOGRAPHY

Arsen Ahmed Mohammed: was born in Kirkuk, Iraq, on 8th Fabriwary, 1985. He received the B.Sc. and M.Sc. degree from the Technical College of Kirkuk University, in 2007, Istanbul University in Electrical and Electronics Engineering, in 2011, respectively. He is currently a lecturer at the Electrical Engineering department of Kirkuk University and He is also a PhD student at Karabuk University. His research interests are active network synthesis, FinFEt transistor.

Hüseyin DEMİREL: graduated from Gazi University Electronic and Computer Education Department in 1997. After thathe received MS and PhD from Gazi University in 1999 & 2010 respectively. As an assistant professor in KarabukUniversity Electrical and Electronic Engineering Department, he is working in digital electronics and thermoelectric modules.

Zaidoon Khalaf Mahmood: was born in Kirkuk, Iraq, on 7th October, 1982. He received the B.Sc. and M.Sc. degree from the Technical College of Kirkuk University, in 2005, Kazan state power engineering University in Electronics Engineering, in 2020. He is currently a lecturer at the University of Kirkuk. His research interests are nano electronics & renewable energy.